Scanning Microscopy

Volume 10 | Number 2 Article 22

5-10-1996

Lectin-Cytochemistry of Experimental Rat Nephrolithiasis

W. C. de Bruijn
Erasmus University, Rotterdam

R. de Water
Academic Hospital, Rotterdam

E. R. Boeve
Academic Hospital, Rotterdam

P. R. W. A. van Run
Erasmus University, Rotterdam

P. J. Vermaire
Erasmus University, Rotterdam

See next page for additional authors

Lectin-Cytochemistry of Experimental Rat Nephrolithiasis

Authors

W. C. de Bruijn, R. de Water, E. R. Boeve, P. R. W. A. van Run, P. J. Vermaire, P. P. M. C. van Miert, J. C. Romijn, C. F. Verkoelen, L. C. Cao, and F. H. Schroder

Scanning Microscopy, Vol. 10, No. 2, 1996 (Pages 557-576) 0891-7035/96$5.00+.25
Scanning Microscopy International, Chicago (AMF O'Hare), IL 60666 USA

LECTIN-CYTOCHEMISTRY OF EXPERIMENTAL RAT NEPHROLITHIASIS

W.C. de Bruijn*, R. de Water[1], E.R. Boevé[1], P.R.W.A. van Run, P.J. Vermaire
P.P.M.C. van Miert[1], J.C. Romijn[1], C.F. Verkoelen[1], L.C. Cao[1] and F.H. Schröder[1]

AEM-unit, Clinical Pathology Institute, Erasmus University, Rotterdam, The Netherlands
[1]Department of Urology, Academic Hospital, Rotterdam, The Netherlands

(Received for publication January 5, 1996 and in revised form May 10, 1996)

Abstract

Lectin reactivity in epithelial apical cell coats of normal rat kidneys was compared to that from animals subjected to crystal inducing diets (CID). The aim was to see whether the absence of lectin reactivity in cell coats is related to intratubular calcium oxalate crystal retention. In normal rat kidneys, after a pre-embedding procedure, it was observed that at the ultrastructural level, reactivity was present but that the lectin specificity for the various parts of the nephron might have to be reconsidered. There was heterogeneity between the epithelial cells with respect to the presence of coat material in the tubular cell apices. Tubular epithelial cell apices from CID rats showed no obvious changes in lectin reactivity pattern. Lectin reactivity was present at the periphery of intratubular crystals but undetectable at true crystal attachment sites or reduced at cell apices in the vicinity of recently attached crystals or agglomerates.

After a post-embedding reaction procedure, wheat-germ agglutinin (WGA)-lectin reactivity confirmed the presence of coat material in the cleft between cell apex and retained crystal at crystal-attachment sites. The WGA/Au-10 nm reaction products were also seen inside epithelial cells. WGA/Au-10 nm reaction products mark a crystal matrix component inside intratubular and retained crystals. A similar matrix was also marked by an α-osteopontin (αOPN/Au-10 nm) reaction product.

Key Words: Nephrolithiasis, rat model, lectin cytochemistry, α-osteopontin immunocytochemistry, reflection-contrast microscopy, electron microscopy.

*Address for correspondence:
W.C. de Bruijn
AEM-unit, Clinical Pathology Institute, Ee902,
Erasmus University Rotterdam, FGG,
P.O. Box 1738,
3000 DR Rotterdam, The Netherlands
Telephone number: 31-10-4087922
FAX number: 31-10-4366660
E.mail: debruijn@pa1.fgg.eur.nl

Introduction

The etiology of human nephrolithiasis has, for years, predominantly been related to the presence of an imbalance between urinary crystal formation and inhibition along the nephron. Contribution to this balance from the tubular lining cells was considered to be restricted to production and excretion of crystallization inhibitors. Rat model systems, in which healthy rats are forced by dietary means to acquire crystals and stones, have frequently been used to obtain detailed information about nephrolithiatic processes hard to acquire from human studies, accepting the risk that processes in humans differ from those in rats [15]. Recent rat-model studies have emphasized a more active role for the lining cells and particularly for their cell-coat material, composed of glycoproteins, in their relation to circulating crystals at their cell apices [3, 13].

Lectins have been used to detect the presence of sugar moieties in the apical cell coats of normal animal and human renal tubular lining cells [32, 68]. Series of lectins, applied to cryostat or paraffin kidney sections, have been claimed to identify the various cell types in certain parts of the nephron by their specific reaction to the cell coat [48, 53, 63]. In experimental nephrolithiasis, selection of a lectin reported to be specific for a certain part of the nephron can assist in cell type characterization, demonstrate cell damage or show where intratubular crystals are present. The lectins known to react with kidney tissue used in the present study are: (a) wheat germ agglutinin (WGA), reported to react with {[(β1-4)D-GlcNAc]$_2$NeuNAc} present in proximal tubules; (b) Dolichos biflorus agglutinin (DBA), reported to react with {D-GalNAc(α1-3)D-GalNAc} present in the loop of Henle and distal tubules; (c) soyabean agglutinin (SBA), reported to react also with {D-Gal NAc(α1-3)D-Gal} present in the loop of Henle and distal tubules and (d) peanut agglutinin (PNA), reported to react with {D-Gal(β1-3)D-GalNAc} present in distal tubules.

Changes in lectin reactivity patterns have been reported on sections from diseased kidneys from either human origin or experimental animal-model systems after

deliberate induction of urothelial cell-coat damage [52, 57]. Nouwen *et al.* [56] demonstrated, after acute damage of proximal tubule cells in gentamicin treated rats, a reduction in PNA, Helix Pomatia and anti-Tamm-Horsfall glycoprotein (αTHP)-reactivity pattern of the distal part of the nephron and restoration during a ten day recovery phase. Gill *et al.* [23] showed that a deliberate acute urothelium damage leading to denuded basement membranes resulted in an increase in calcium oxalate monohydrate (COM) crystal retention.

In a recent series of papers, we have described the process of exotubulosis in a rat nephrolithiasis model [3, 13, 14, 16, 17]. In this model, intratubular crystals are induced by a drinking-water regime on ethylene glycol (EG) plus ammonium chloride (AC), {crystal induction diet (CID) = CID^{AC}}, followed by a 1-3 day post-induction recovery phase (PIR) on normal drinking water. A similar process of crystal induction has been observed in rats after a CID of EG plus vitamin D_3 (CID^{VitD}) or a stone inducing diet (SID^{AC}) [16, 17]. In these studies, intratubular crystals have been noticed to be retained by epithelial cellular apices. Since the apical cell coat is likely to be involved in this retention process, we propose to apply lectin detection reactions to visualize coat materials. Previously, it has been attempted to visualize the presence of a proximal cell coat by application of an alkaline-phosphatase reaction in a pre-embedding procedure [14]. But lectins are more appropriate to demonstrate the presence of various coat materials along the whole nephron and also because enzyme losses have been reported during CID [27]. To which degree this retention process contributes to nephrolithiasis [21, 26, 38, 40, 41] remains to be further investigated. But it is realized that when the retention process does contribute, the process may be determined by, e.g., the absence of cell coat material. This paper deals with the first two steps in this event: crystal retention on cell apices and the role of coat materials and the overgrowth of the retained crystal by neighboring epithelial cells, leading to exotubulosis. It was also attempted to restore anticipated cell coat damage from CID by concomitant oral intubation of synthetic sulphated poly-saccharide (G872) derived from seaweed. For details about the effects of G872 on crystal growth and agglomeration, see [4, 6, 7]. Positive effects of the application of glycosaminoglycans (GAGs) have also been reported for bladder epithelial surfaces, where GAGs appear to restore damage and to decrease crystal retention [23, 52, 57, 58].

To technically demonstrate lectin reactivity, we chose: (1) a pre-embedding procedure that allows the observation of lectin reactivity at the ultrastructural level, since reaction sites are located extra-cellularly; (2) a post-embedding procedure in Lowicryl K4M-resin (Balzers/Pfeiffer, Maarssen, The Netherlands) for possible Pre-embedding procedure on Vibratome sections.

Figures 1 through 8 from **untreated and CID^{AC} rats.**

Figures 1 through 4 show cell-coat-related reaction products, seen by RCM as an increase in intensity, after single-lectin incubation at 4°C. Detection: $PO/Os^{VI}Fe^{II}$ without H_2O_2 blocking of endogenous PO. Bar (in Fig. 1) = 10 μm; Figures 1-4 are at the same magnifications.

Figure 1. Cell-coat reactivity for SBA in the papillary region from normal rats. **Figure 2.** Cell-coat reactivity for PNA in the papillary region from normal rats.

Figures 3 and 4 show cell-coat-related reaction products, from rats after CID^{AC}.

Figure 3. Cell-coat reactivity for DBA is shown in the papillary region. Note the heterogeneity of the apical reaction (arrow), the staining of some capillaries and absence of staining in more proximal tubules. **Figure 4.** WGA cell-coat reactivity in the cortical region.

---

intra-cellular or intra-crystalline localizations and (3) pre- and post-embedding procedure combinations with two different markers.

In the pre-embedding procedure, biotinylated lectins were applied to 100 μm thick sections from paraformaldehyde or glutaraldehyde perfusion-fixed rat kidneys. After the peroxidase-conjugated lectin-detection step, this was combined with a previously described [8] post-fixation procedure with ferrocyanide-reduced OsO_4 for ultrastructural observation [9]. In the post-embedding procedure, 100 μm thick untreated or pre-treated Vibratome sections from the same kidney were embedded in Lowicryl K4M at -20°C according to Zondervan *et al.* [75], and similar lectin-detection reactions were performed on thin sections. Results from our preliminary studies to determine lectin reactivity in relation to the type of aldehyde fixation did not show any difference. Selectivity and specificity test results of the chosen detection procedure and sugar-blocking reactions published by others [68] will not be included in this study. The procedures proposed provide optimal results with respect to the preservation of ultrastructure, crystals and crystal matrix interactions [14, 34-43]. The lectin reaction products created were visualized by a combination of light microscopy (LM), namely, reflection-contrast light microscopy (RCM), and energy-filtered transmission electron microscopy (EFTEM). Recently, similar stimulating results have been obtained by Prins *et al.* [59] with the use of a combination of RCM and conventional TEM. Results from crystal and cell interactions with αTHP glycoproteins are shown elsewhere [19].

The questions to be answered are:

(1) Can we confirm cell-coat material detection at

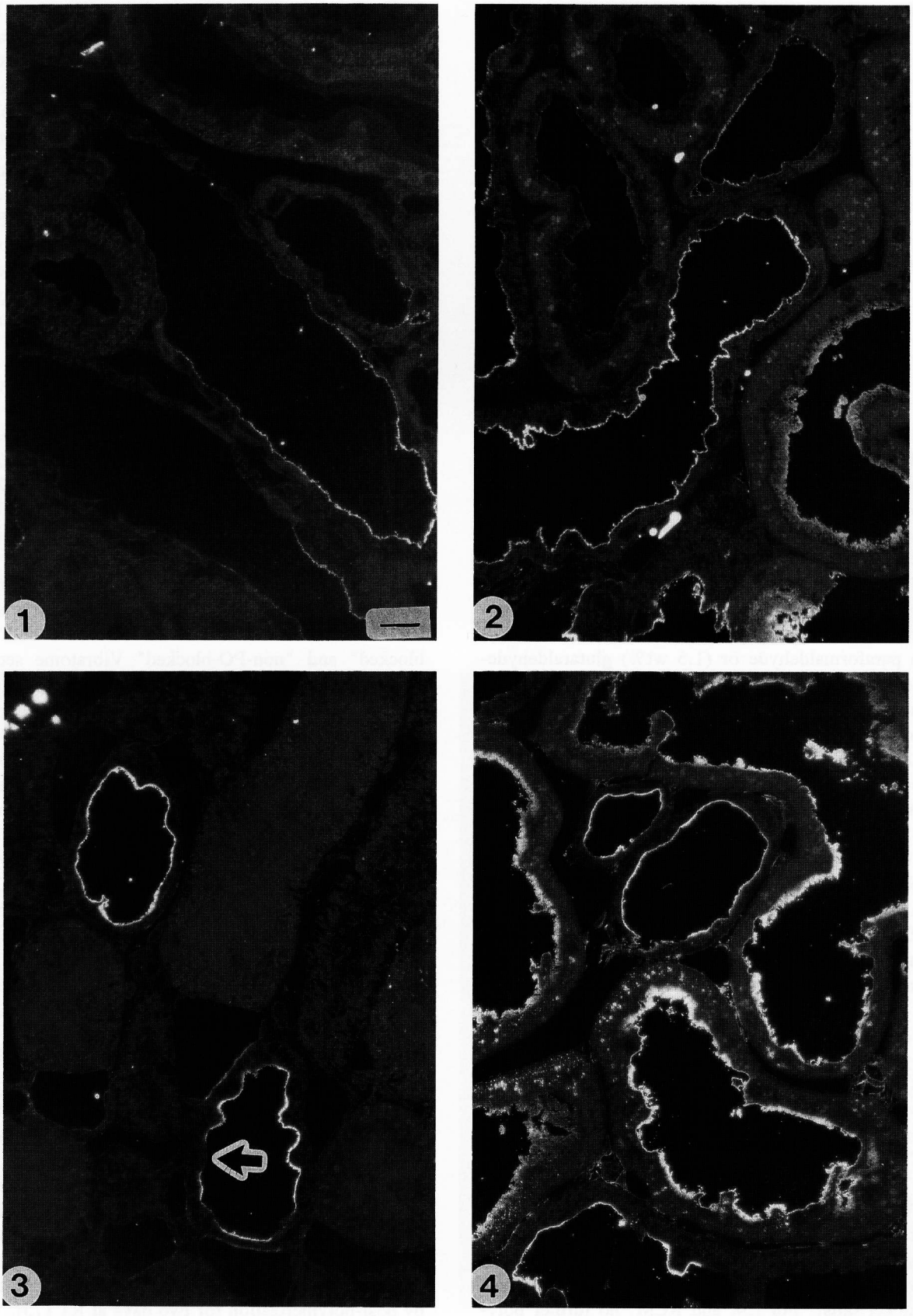
1
2
3
4

the apex along the nephron in normal rats while preserving the ultrastructure?

(2) Can cell coat material be detected at the apex of all cells? Is that cell-coat distribution pattern influenced by CIDs?

(3) Is coat material present in the cleft between the crystal and the cell apex at crystal-attachment sites and can it be visualized at the ultrastructural level?

(4) Do detectable cell-coat changes interfere with the process of crystal retention?

(5) Can lectin reactivity be detected inside lining cells at the ultrastructural level?

(6) Can lectin reactivity be used to characterize a matrix inside intra-tubular or retained crystals or crystal agglomerates?

Material and Methods

The animal model and the way crystals are induced by an EG diet, either CID^{AC} or CID^{VitD}, have been described before [3, 13]. In some animals, the assumed damaging effects of crystal induction by CID^{VitD} were counteracted by an oral intubation with the compound G872 derived from seaweed in a dosage of 10 mg/kg-body-weight every day for 30 days. For details about G872, see references [4, 6, 7]. From segments of (4 wt%) paraformaldehyde or (1.5 wt%) glutaraldehyde-perfusion fixed rat kidneys, 100 μm thick Vibratome (Cambridge Instrument, London, U.K.) sections were obtained. All sections were quenched in 0.5 M AC for 30 minutes at 4°C, and after rinsing with 0.1 M phosphate-buffered saline (PBS) of pH 7.2 containing 0.1 vol.% Triton (TPBS) (Merck, Damstadt, Germany), were incubated for 18 hours at room temperature (RT) or at 4°C, with the respective dilutions of the lectins in TPBS {0.02% TPBS + 1.5 wt% bovine serum albumin (BSA; from Organon, Oss, The Netherlands}.

The biotinylated lectins (Vector Laboratories, Inc., Burlingame, CA) used were: WGA, DBA, SBA, PNA {all in dilutions (1:300)} and a mixture of all four lectins (each diluted 1:300), thus obtaining maximal coat reactivity, but sacrificing lectin specificity. Biotinylated sections were treated with peroxidase-conjugated streptavidine (Biogenex, San Ramon, CA) for 3 hours at RT and infiltrated with diaminobenzidine tetrachloride (DAB) (Fluka, Bornum, Belgium) without H_2O_2 for 10 minutes at RT. The peroxidase activity was developed with a reagent (Pierce Product No. 34065, Omnilabo Intl., Breda, The Netherlands) containing DAB and a stable peroxide buffer by incubating the sections for 10 minutes at RT in the dark. The poly-DAB reaction product visualized by this reagent includes poly-DAB staining cobalt and nickel salts. For LM and RCM, no further poly-DAB staining is used. Two types of pre-embedding blank reactions were performed: reagents deprived of lectins or streptavidine.

In peroxidase (PO) procedures, a blocking reaction for endogenous PO activity (1 vol% H_2O_2 in 70% ethanol for 1 hour at RT) is generally recommended to be performed directly after the quenching step. This blocking procedure was tested on Vibratome sections in two ways: (a) its interference with the presence of crystals; here it was found that the blocking procedure did not reduce crystal bi-refringence and (b) membrane preservation at the ultrastructural level. We used both "PO-blocked" and "non-PO-blocked" Vibratome sections. Provided the risk of false-positive PO reaction sites can be accepted, we advocate the omission of this blocking step because it reduces the OsO_4-reactivity of cellular membranes. Endogenous PO reactivity resulting in monocyte and granulocyte granule staining is appreciated because it assists in the characterization of inflammatory cells.

Some Vibratome sections were subsequently post-fixed with 1 wt% OsO_4 (in 0.1 M cacodylate/HCl buffer, pH 7.4) which was reduced by the addition of $K_4Fe^{II}(CN)_6 \cdot 3H_2O$ to a final concentration of 0.05 M [8, 9] for 1 hour at RT. This reaction creates membrane and glycogen contrast, and also intensifies lectin/PO reaction products (lectin/PO/$Os^{VI}Fe^{II}$). In some cases, PO reactivity was amplified with $K_2PtCl_6 \cdot 2H_2O$ [12, 30].

All Vibratome sections were dehydrated in a graded acetone series, infiltrated with epoxy resin and finally flat embedded in epoxy resin, which was polymerized for 18 hours at 60°C. Alternatively, untreated or lectin/PO pre-treated Vibratome sections and 1 mm thick slices were dehydrated by a progressive lowering of temperature technique for K4M embedding in a Balzers TTP-010 unit (Balzers/Pfeiffer). Polymerization at -20°C for 24 hours under ultraviolet light was followed by post-polymerization for two days at RT [75]. From blocks, 1 μm thick LM and 0.2 μm thick RCM sections,

In **Figures 5 and 6**, electron micrographs show lectin/PO/$Os^{VI}Fe^{II}$ reaction products in tubular cell apices after single lectin incubation at 4°C without H_2O_2 blocking of endogenous PO from normal control rats. **Figure 5**. A black SBA reaction product. **Figure 6**. A PNA reaction product and its absence in an adjacent tubule.

In **Figures 7 and 8**, electron micrographs show the lectin/PO/$Os^{VI}Fe^{II}$ reaction products in tubular cell apices from rats after CID^{AC}. Single lectin incubation. **Figure 7**. A distribution of SBA reaction product. Note the heterogeneity in apex staining between neighbouring cells. Figure 7 is at the same magnification as Figure 6. **Figure 8**. A distribution of WGA reaction product.


5
<-->2.5μm


6
<-->1.7μm

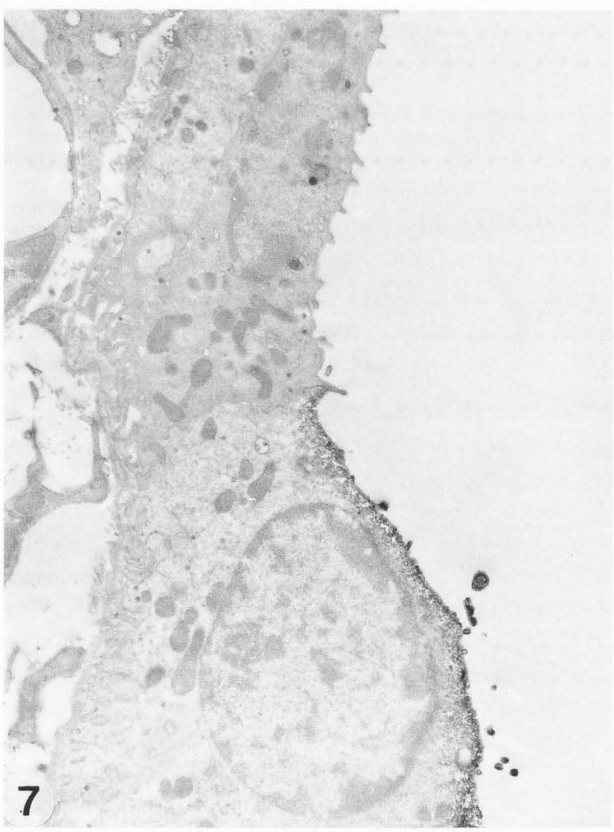
7

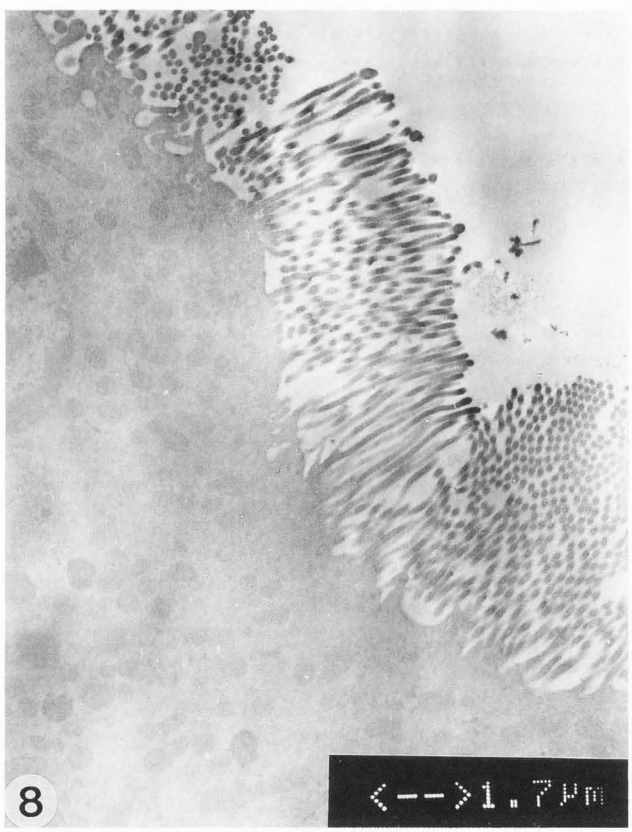
8
<-->1.7μm

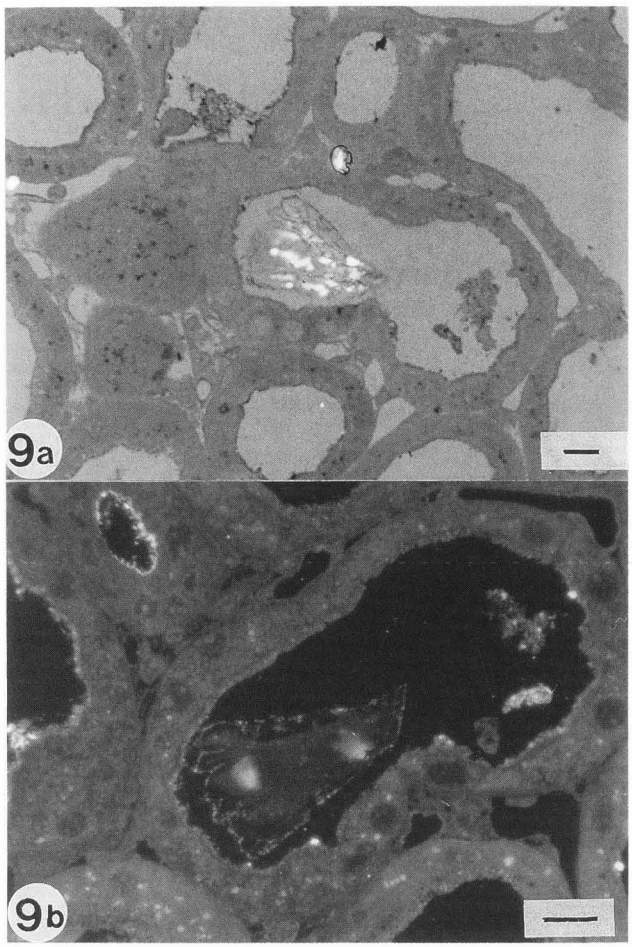

Figures 9 and 10 show LM and RCM images. **Figures 11, 12 and 13** show TEM images from rat tissues after **CID^{AC} plus PIR**. Pre-embedding procedure with Mix4/PO. Detection: PO/$Os^{VI}Fe^{II}$, without H_2O_2-blocking.

Figure 9. LM crystal appearance and cell-coat reactivity from a 1 μm thick LM-stained section under crossed Nicol prisms (a) with the unstained adjacent 0.1 μm thick section in RCM (b). Bars = 10 μm. **Figure 10**. Cell-coat reactivity of Mix4/PO reaction product around a large just-retained crystal and a crystal completely surrounded by epithelial cells (*). Note the relative absence of coat material below the crystal and the absence at the basis of the crystal after exocytosis and the presence of intratubular cells. This figure is at the same magnification as Figure 9b.

---

acquired with a glass knife on an LKB Ultrotome V and collected on glass slides, were either stained with Toluidine Blue (LM) (Nustain, Nottingham, U.K.) or left unstained (RCM). The 50 nm thick ultrathin sections were acquired with a diamond knife (Diatome, Biel, Switzerland) on an LKB Ultrotome V (LKB, Lana, Sweden) and collected on Formvar (TAAB-Laboratories Equipment Ltd., Aldermaston, Berkshire, U.K.)/carbon-coated copper one-hole grids or on 400 mesh copper grids with or without a Formvar film. Section staining (with uranyl acetate and/or lead citrate), which improves cellular contrast, was omitted because it removed preserved crystalline material at the cost of impaired ultrastructural visualization, which is compensated for by the use of EFTEM [66]. The post-embedding lectin-staining procedures for Lowicryl sections for LM and RCM were identical to pre-embedding lectin/PO procedures of the Vibratome sections. For the post-embedding ultrastructural lectin-staining of Lowicryl sections and those of the combined procedures, a colloidal gold protocol was applied: section-containing grids were rinsed for 3 minutes in 0.1 M PBS of pH 7.2, incubated with biotinylated lectins (1:300 + BSA 0.5 wt% in PBS) for 18 hours at 4°C and rinsed for 10 minutes in PBS. Subsequently, sections were incubated in anti-biotin/Au-10 nm (1:20 in PBS + 0.5 wt% BSA; Aurion, Wageningen, The Netherlands), rinsed in PBS and for 3 minutes in Millipore-filtered water {(Milli Q) Millipore Corp., Bedford, MA}

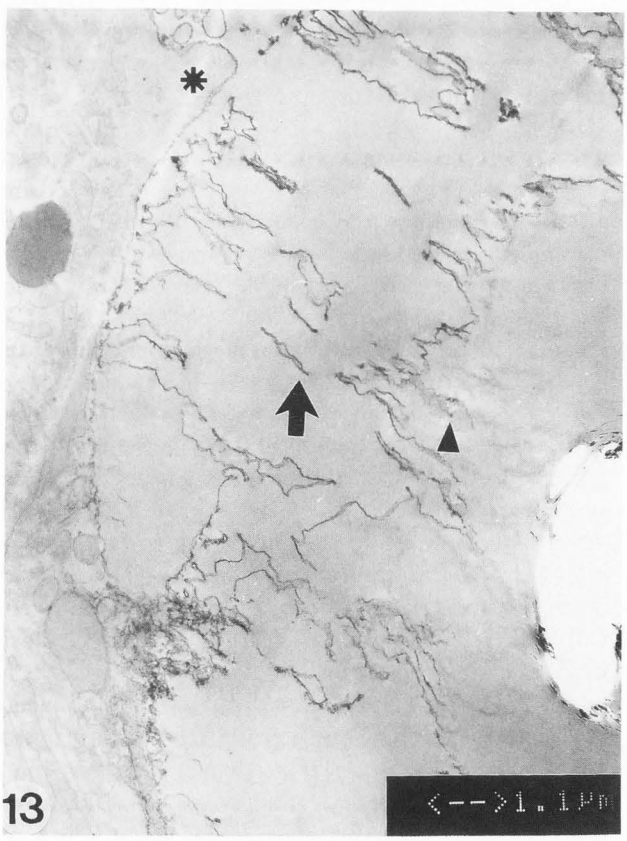

Figure 11. Pre-embedding procedure, with WGA/PO/ $Os^{VI}Fe^{II}$ (with H_2O_2 blocking of endogenous PO) shows a preserved 2 μm-sized crystal at a faintly-marked villous apex.

Figure 12. Vibratome section incubated in Mix4/PO (without H_2O_2 blocking). The reaction product is present on the villi above and below the attachment place of a retained large crystal. The preserved crystal remainder is not included in this image.

Figure 13. Vibratome section incubated in Mix4. The reaction product is present at the free cell surface (*) but absent at the attachment place of the retained large crystal. The crystal remainder is included and unstained (arrowhead) and contrasted parts of the crystal interior are indicated (arrow).

---

at RT and air dried.

For the reaction with αOsteopontin (αOPN) (ultra)thin sections were incubated with mouse-αratOPN (1:7000, in PBS of pH 7.2 + 0.5 wt% BSA) for 18 hours at 4°C (the mouse-αratOPN was obtained from the Developmental Studies Hybridoma Bank, Dept. Pharmacology and Molecular Sciences, Johns Hopkins Univ. Sch. Med., Baltimore, MD). The sections were rinsed with TPBS (0.1 vol% in PBS) and pre-incubated

with normal goat serum (NGS, 1:10 in TPBS 0.02% + BSA 1.5 wt%) (Dako, Glostrup, Denmark) for 30 minutes at RT. Sections that had not been rinsed were treated with a biotinylated goat multi-linker (1:50 in PBS + 0.5 wt% BSA) (Biogenex) for 3 hours at RT and rinsed in TPBS 0.1% (Biogenex), incubated in streptavidin/Au-10 nm (1:20 in PBS + 0.5 wt% BSA) (Aurion), rinsed in PBS, soaked 3 minutes in Milli Q at RT and air dried. For RCM visualization, sections were reacted with Biogenex streptavidine/PO as described for the pre-embedding procedure. In blank reactions, the primary antibody was replaced by PBS or a non-specific antibody-incubation or the multi-linker was omitted.

Images from the LM and RCM sections were recorded with a Zeiss Axiophot (Zeiss, Weesp, The Netherlands) on Kodak TMX 100 film (Eastman Kodak, Rochester, NY). The ultrathin sections were recorded in a Zeiss EM 902 TEM (Zeiss, Oberkochen, Germany) on Agfa Scientia EM sheet film (Agfa, Antwerpen, Belgium).

Results

Pre-embedding procedure with single lectins in normal and CID^{AC} rats

In Figures 1 through 8, cell-coat material is detected by RCM and TEM.

In Figures 1 and 2, cell-coat reactivity for SBA/PO (Fig. 1) and PNA/PO (Fig. 2) after reaction with reduced osmium was shown in the papillary region of a normal rat kidney. The presence of a coat reaction product in some tubules and the well preserved kidney and mitochondrial architecture were clearly visible. Similarly, DBA/PO and WGA/PO incubations showed reaction products along cells in other parts of the nephron (not shown).

In Figures 3 and 4, cell coat specificity in rats after a CID^{AC} was demonstrated for the lectin DBA/PO in Figure 3 and for WGA/PO in Figure 4. Positively and negatively marked cell apices were present next to each other.

Figures 5 and 6, contrasted by a reduced osmium reaction, transmission electron micrographs show the presence and absence of the various reaction products in normal rat tubular cell apices in combination with cellular ultrastructure. Parallel to Figures 1 and 2, Figure 5 shows the SBA and Figure 6, the PNA reactivity. In rats, given a CID^{AC}, Figure 7 shows the SBA positive and negative cell-coat material in neighbouring cells; Figure 8, that for WGA positive sugars. EFTEM was unable to detect the presence of either cobalt or nickel in the contrasted reaction products. In the blank reactions, with omission of a biotinylated lectin or streptavidine step, coat staining was not observed.

Figures 14 through 16, pre-embedding procedure on sections from **G872-treated CID^{vitD} rats**. WGA/PO/$Os^{VI}Fe^{II}$ reactivity (with H_2O_2 blocking) detected by LM (insets) and TEM. Figures 14, 15 and 16 are at the same magnification (see below for insets). **Figure 14.** WGA/PO/$Os^{VI}Fe^{II}$ reaction product in the tubular cell apices, around the stalk and partially at the crystal surface (**inset**; inset bar = 50 μm). Its presence (arrow) is confirmed in the electron micrograph from the rather well preserved crystal mass. **Figure 15**. Transmission electron micrograph shows the WGA/PO/$Os^{VI}Fe^{II}$ reaction product on the cell apex (arrow) and on the crystal surface (*). Between the preserved crystals and the crystal coat matrix, material is contrast stained by the post-fixation reaction. **Figure 15, inset**: The localization of the WGA/PO/$Os^{VI}Fe^{II}$ reaction product in the cell apices, is less outspoken in this tubule (inset bar = 20 μm). **Figure 16**. The localization of a WGA/PO/$Os^{VI}Fe^{II}$ reaction product in cell apices (arrow) at this attachment site is continuous with the small apical part of the free-crystal surface. The crystal base has no reaction product and lacks an internal matrix.

Pre-embedding procedure with lectin mixtures in CID^{AC} rats

Vibratome kidney sections from CID^{AC} rats were incubated with a lectin mixture consisting of (WGA + SBA + PNA + DBA)/PO (Mix4/PO). In normal rat kidney Vibratome sections treated with Mix4/PO/$Os^{VI}Fe^{II}$, virtually all cell apices were contrasted, but the mentioned heterogeneity is still present (not shown). Figures 9 and 10 show RCM and LM images. To compare the appearance of the crystalline material in RCM, the same sites are shown in two adjacent sections. Figure 9a shows the conventional LM under crossed Nicol prisms and Figure 9b shows the RCM image. The cell coat material in the surroundings of the crystal is weakly positive for the lectin/PO mixture. In Figure 10, a crystal attached at one point to the cell coat is shown. The apices nearest to the crystal are less contrasted by Mix4/PO. The opposite site of the crystal and the apices facing that site are stained. Also, inside the crystal, an irregular staining pattern is seen. Single cells were seen to be attached to the crystal surface. A crystal is seen partially overgrown by epithelial cells with a lectin/PO positive cell coat (*). The exotubulosis process is almost finished, the intimate cell-crystal contact at the basis is unstained and the crystal apex facing the lumen is stained. The electron micrographs, Figures 11, 12 and 13, show crystal attachment sites. In Figure 11, a preserved 2 μm crystal is seen at the villous apex of a cell faintly marked with WGA/PO material in a situation which may reflect a first encounter. In Figure

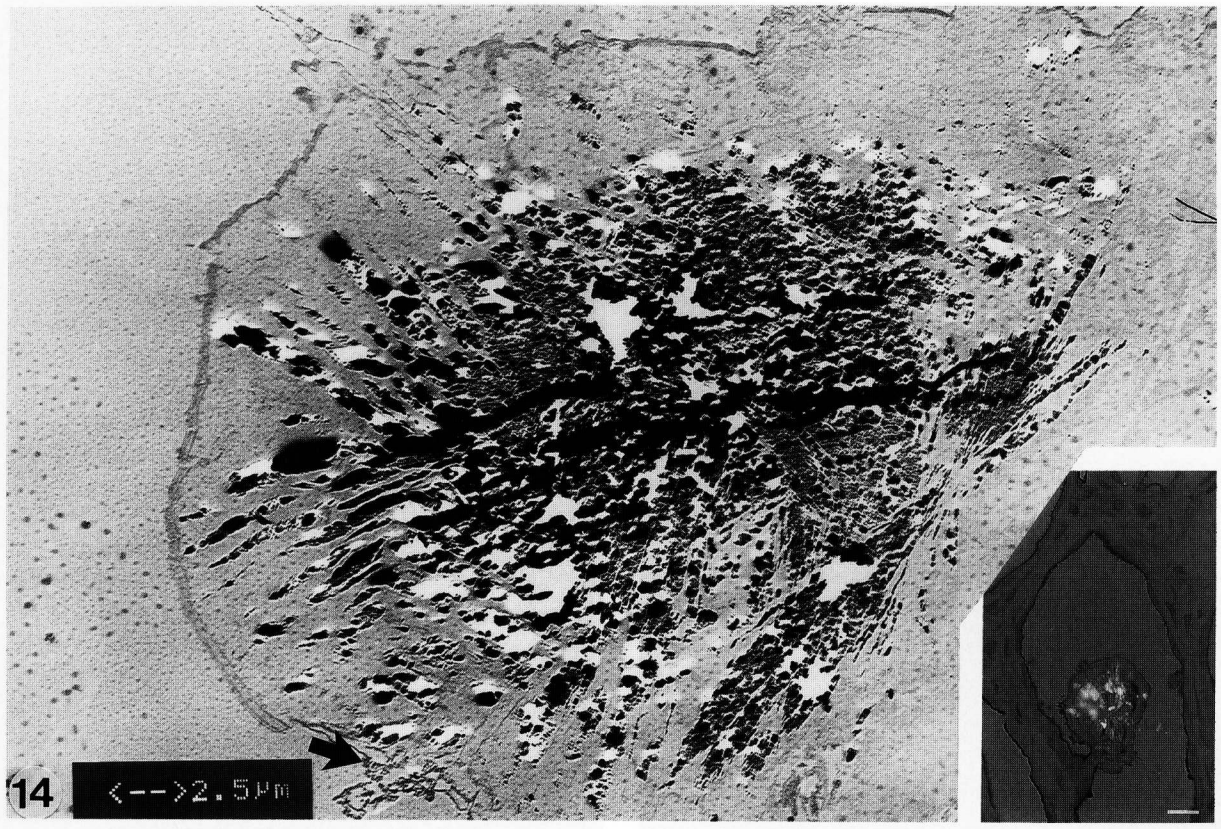
14
<--->2.5μm

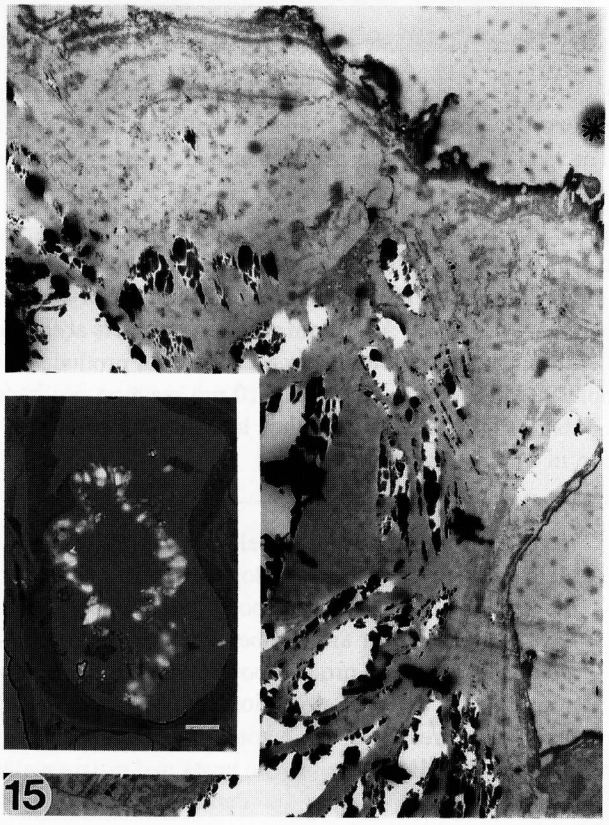
15

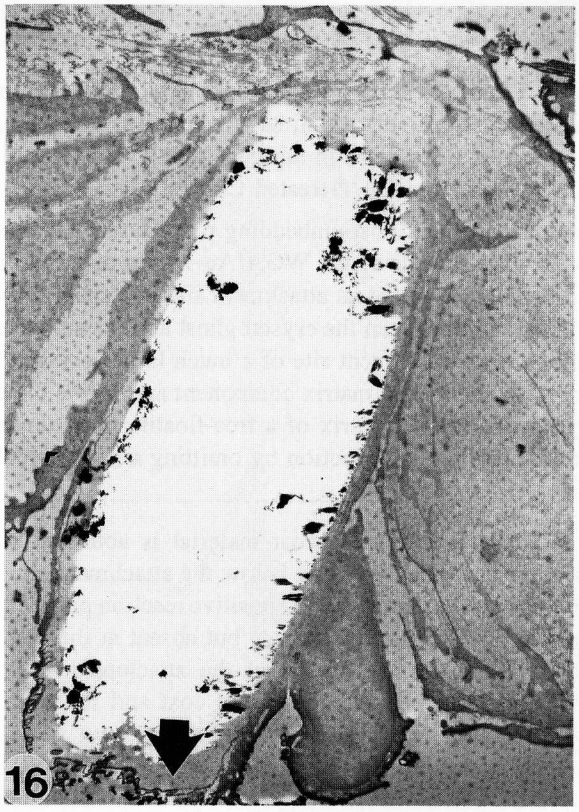
16

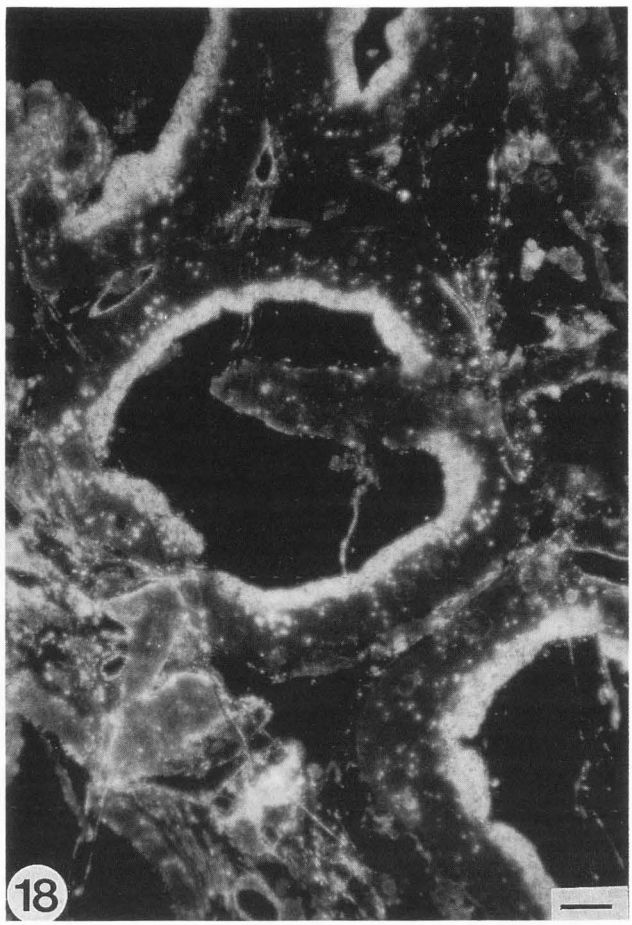

Figures 17 and 18 show the intensity increase in RCM images after a post-embedding WGA/PO reaction. Both figures are at the same magnification; bar (in Fig. 18) = 10 μm. **Figure 17.** In control rats, an area with abundantly stained and unstained cell apices in adjacent tubuli. **Figure 18.** The WGA/PO reaction product in cell apices, around and inside crystals from G872-treated CID^{vitD} rats.

Combined Pre- and Post-embedding procedure. **Figures 19, 20, 21 and 22 (on the facing page)** show transmission electron micrographs of the WGA/Au-10 nm reaction product in CID^{AC} rat without pre-embedding reaction. **Figure 19.** Lectin reactivity at an attachment site of a small crystal ghost in the cytoplasm, at the periphery of the crystal ghost and in the cleft between the crystal ghost and the cell apex. **Figure 20.** WGA/Au-10 nm reaction products at the same locations at an attachment site of a much larger crystal. In addition, it shows the presence of reaction products inside the crystal, marking a matrix component and inside the cytoplasm. **Figure 21.** WGA/Au-10 nm reaction products in a crystal, marking a matrix of a free-floating intratubular crystal. **Figure 22.** The rather low number of Au-10 nm particles after a blank reaction by omitting a WGA incubation in a retained crystal.

12, Mix4/PO positive cell-coat material is abundantly present on the villi above and below the attachment site of the crystal. Lectin-Mix4/PO positive reaction product is present at the crystal periphery but absent at the cell surface underneath the crystal at the attachment site. The relation between the apical cell coat and the coat material around the crystal becomes closer at a place where the microvilli have partially disappeared. Inside the crystal, a lectin-Mix4/PO reaction product pattern is seen to be continuous with the coat at the crystal periphery. In Figure 13, the lectin-Mix4/PO negative attachment zone is extended and cell debris is present in the cleft between crystal and cytoplasm. The free part of the cell is lectin-Mix4/PO positive, even though villi have disappeared or are clubbed (*). Inside the crystal, a lectin/PO reaction product positive pattern is seen radiating toward the central portion where some crystalline material is preserved. In a zone immediately surrounding the crystalline material, the unstained matrix material (arrowhead) is seen to be continuous with a more peripheral contrasted part (arrow).

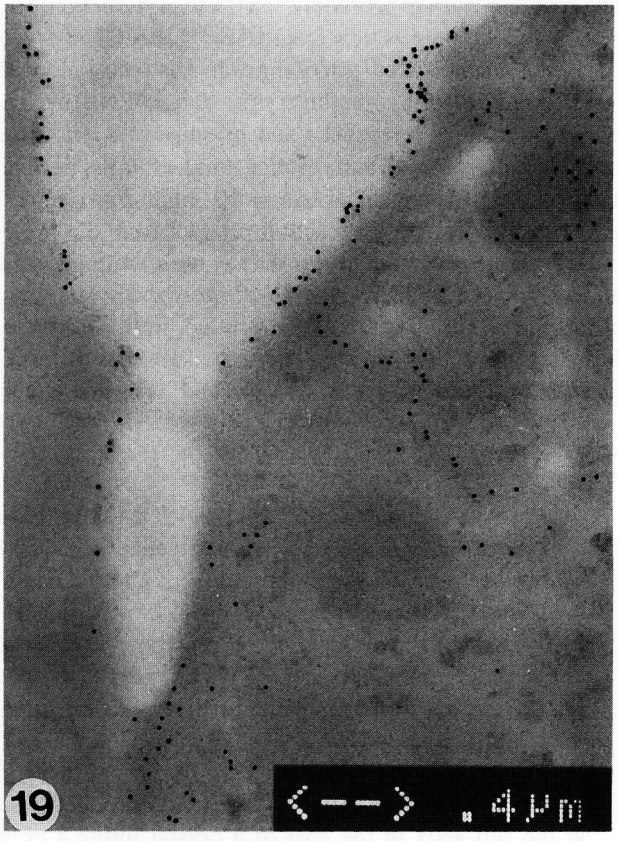
19
<--> .4µm

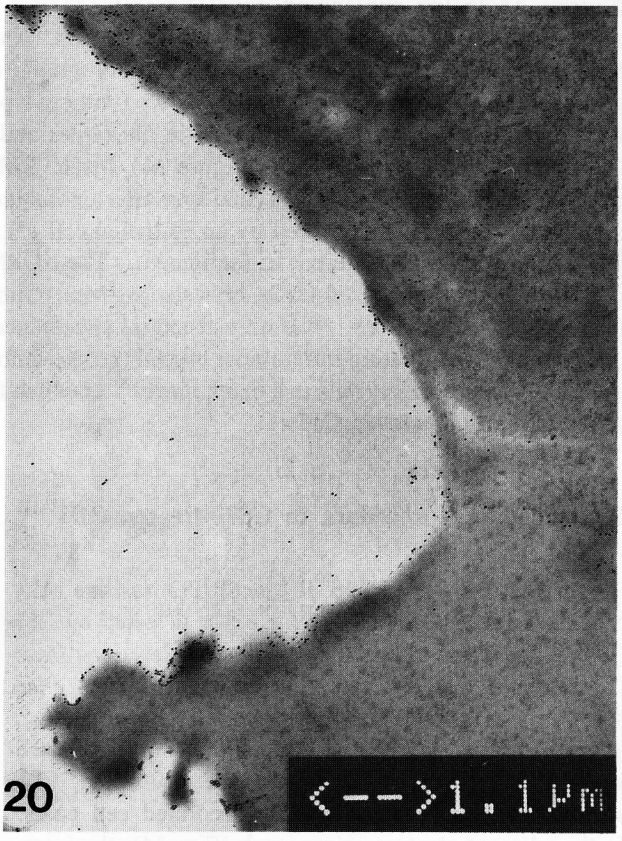
20
<-->1.1µm

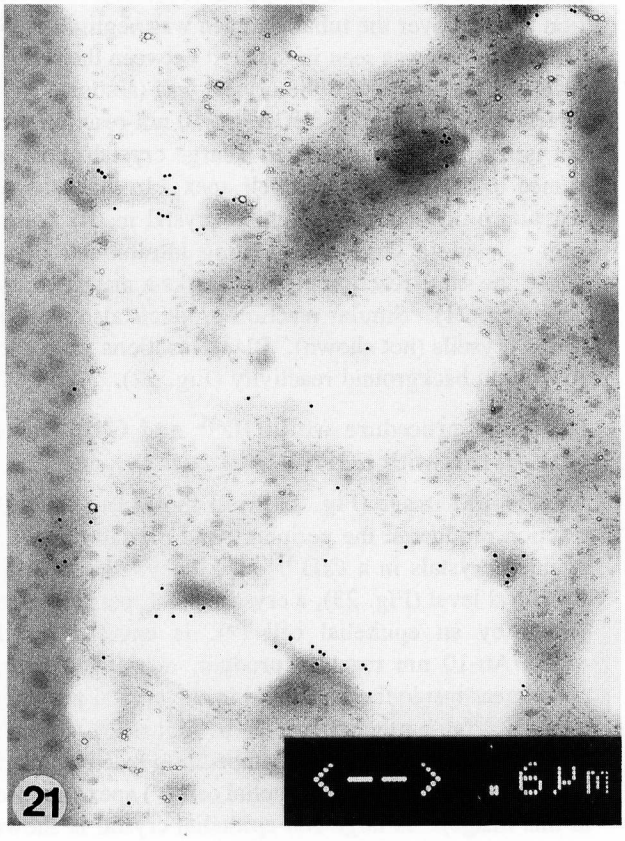
21
<--> .6µm

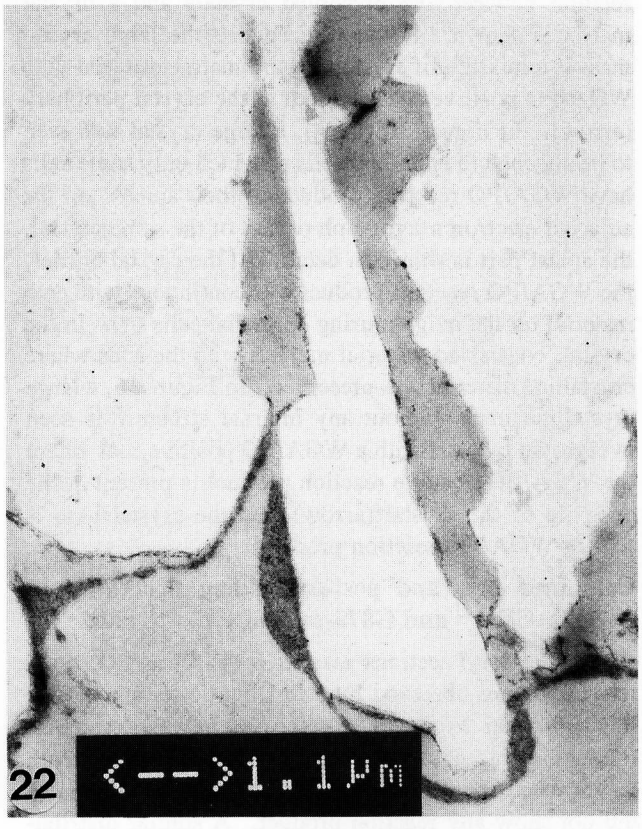
22
<-->1.1µm

Figures 23-26 (on the facing page). Combined Pre- and Post-embedding procedure on Lowicryl sections from **untreated, CID^{AC} and G872-treated CID^{vitD} rats.** The αOPN/Au-10 nm-reaction from **CID^{AC} and G872-treated CID^{VitD} rats. Figure 23.** In this electron micrograph, αOPN/Au-10 nm-related reaction product is seen in a crystal ghost just below the epithelial cell (*) surface (without a pre-embedding reaction). In the crystal, the αOPN/Au-10 nm-related reaction product is seen located in the center and in the margin between crystal and its surroundings. Figure 23 is at the same magnification as Figure 24. **Inset:** LM image of αOPN/Au-10 nm reaction product at the periphery of a retained crystal (*) and a second one after exotubulosis in the interstitium (inset bar = 10 μm). **Figure 24.** A similar attachment zone covered by an epithelial cell (*) marked by a WGA/PO/Pt reaction product from the pre-embedding treatment (not present in the image). The αOPN/Au-10 nm-related reaction product is seen around partially preserved micrometer sized CaOx crystals (arrows). Similar products can be seen around 100 nm-sized crystal ghosts (arrowhead). **Figure 25.** The ultrastructural appearance of an αOPN/Au-10 nm-reaction product in the matrix of a ghost from a free-floating intratubular crystal (no pre-embedding reaction). **Figure 26.** The virtual absence of reaction product over similar crystals in a blank reaction in which the αOPN incubation step has been omitted. The arrow points to the partially preserved CaOx.

Pre-embedding procedure in G872-treated CID^{VitD} rats

In Figures 14, 15 and 16, lectin/PO positive cell-coat material (WGA/PO/$Os^{VI}Fe^{II}$) was detected by LM (insets) and TEM in rat kidney Vibratome sections from G872-treated CID^{VitD} rats. In Figure 14 (inset), the specificity of the WGA/PO for these cell apices is shown at the LM level. Epithelial WGA/PO positive cells are seen in the stalk where the crystal mass is attached. The surrounding apices show heavily decorated cell coats. In the adjacent electron micrograph (Fig. 14), the inter-relation between the preserved crystals and a crystal matrix is shown. It was noticed that the large crystal mass is a mixture of crystalline and matrix material with WGA/PO positive coat material at the crystal periphery (arrow). In Figure 15 (inset), a large crystal was seen to be attached to epithelial cells of which only some cells have WGA/PO reaction product on their apices. In the adjacent electron micrograph of part of the same crystal, the apical part is shown in detail. At the crystal border, the WGA/PO reaction product was continuous with coat material on the neighbouring epithelial cells (*). In the crystal, contrasted material merged with the sites where crystalline material was preserved. In Figure 16, a large crystalline mass without any internal structure is seen overgrown by cells with a WGA/PO positive coat where the WGA/PO positive reaction product is present at the open tip of the crystal (arrow), but the crystal base is free of WGA/PO reaction product.

Combined pre- and post-embedding procedure in normal, CID^{AC} and G872-treated CID^{VitD} rats

In Lowicryl sections reacted with lectins/PO, reactive sites were observed by RCM due to its increase in intensity. In Figure 17, WGA/PO positive reaction product is present in proximal epithelial cell apices from an untreated control rat. Adjacent, non-proximal tubules did not show any reaction product. A similar distribution pattern is seen for PNA/PO and DBA/SBA/PO reactivity in more distally located segments (not shown). The reaction product distribution from CID^{AC} rats was similar to that in control animals. G872-treated CID^{VitD} rats (Fig. 18) showed WGA/PO reactivity in a crystal-containing proximal segment in which, next to the brush border reactivity, a WGA/PO positive reaction product was also seen inside the crystals.

In electron micrographs from CID^{AC} kidneys, the presence of a WGA/Au-10 nm reaction product is seen at the cell apex in the coat of a crystal lining a crystal ghost and at sites in the cytoplasm (Fig. 19). The reaction product over the tubular lumen was negligible. Reaction product was seen in the cleft between the cell surface and the site where the crystal was (assumed to be) attached. In Figure 20, WGA/Au-10 nm-reaction product is seen at similar sites in a large crystal ghost (assumed to be) attached to a cell apex. In this case, the reaction product marks a similar crystal matrix component. Inside a large free-floating intratubular crystal ghost, the same reaction product marks a matrix component (Fig. 21). Similar reaction products also mark retained crystals (not shown). Blank reactions gave a low Au-10 nm background reactivity (Fig. 22).

Combined procedure with CID^{AC} and G872-treated CID^{VitD} rats with αOPN

The LM image (Fig. 23 inset) shows an αOPN-PO reaction product at the periphery and partially inside in retained crystals in a CID^{AC} rat kidney. At the ultrastructural level (Fig. 23), a crystal ghost, partially overgrown by an epithelial cell (*), is covered by the αOPN/Au-10 nm reaction product, marking a matrix component inside the ghost and in the crystal periphery towards a sub-epithelial space. In Figure 24, a similar situation is shown after a pre-embedding reaction, marking a WGA/PO positive epithelial cell (*) apex (not seen in this image). A large sub-epithelial crystal is shown

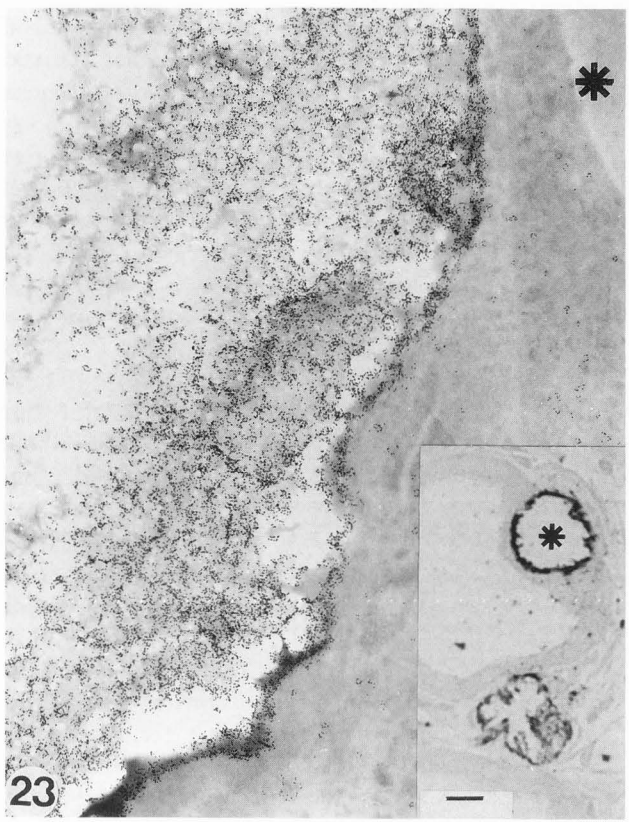
23

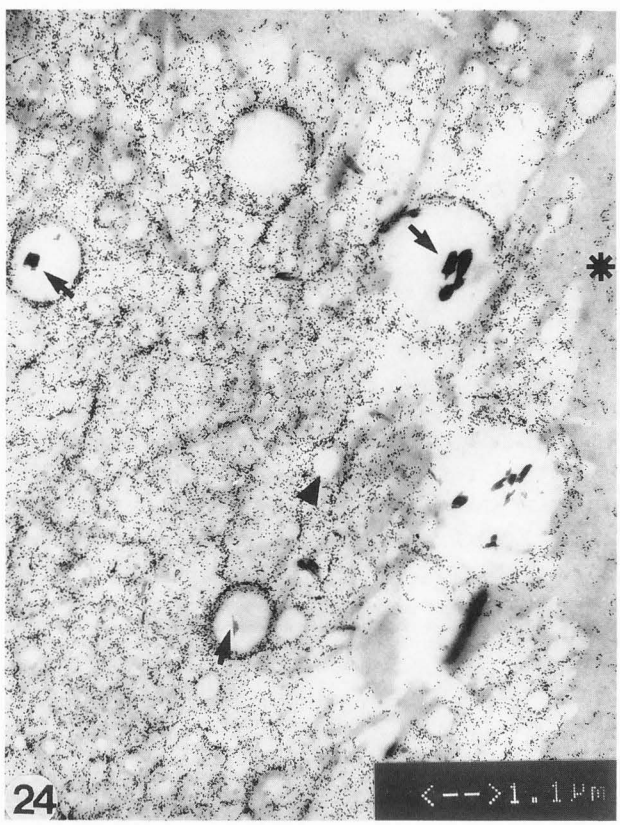
24
<--->1.1µm


25
<--> .6µm

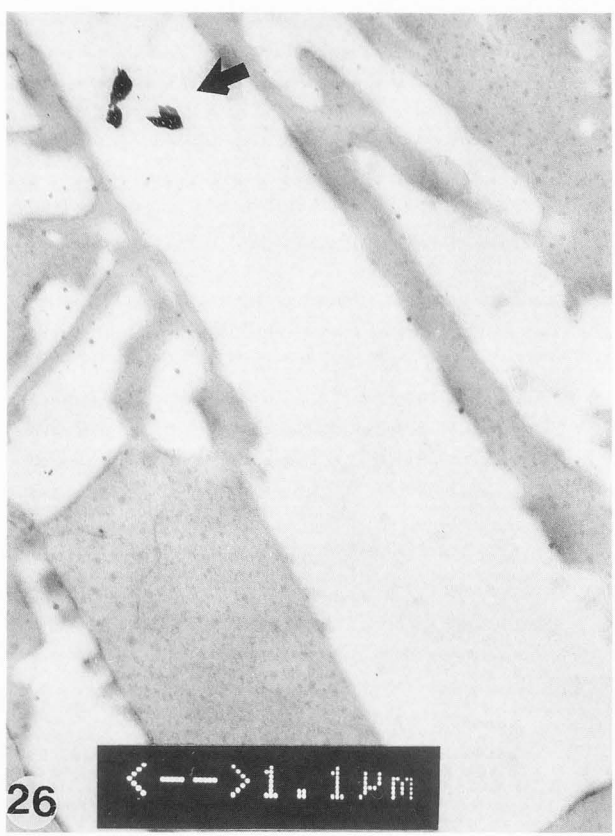
26
<--->1.1µm

with αOPN/Au-10 nm reaction products. Inside the crystal, reaction product is seen around μm-sized, partially preserved crystals (arrows) and around about 100 nm-sized crystal ghosts (arrowhead). In Figure 25, the post-embedding αOPN/Au-10 nm reaction product is seen inside a free-floating intratubular large crystal, marking a crystal matrix component in a G872-treated CID^{VitD} rat. Figure 26 shows, in the same CID^{AC} rat kidney after a blank reaction without antibody, the virtual absence of a positive reaction product inside a retained crystal in which part of the CaOx material is preserved (arrow).

Discussion

In this study, as an answer to questions (1) and (2), combined LM, RCM and TEM observations show that:

(a) Cell membrane-bound coat material can be detected at the extracellular site of the epithelial cells along the nephron. Ultrastructural details are preserved in ultrathin sections from kidneys treated with a lectin/PO/$Os^{VI}Fe^{II}$ procedure.

(b) The specificity of lectin reactivity for sugar moieties in the various nephron parts is observed. But cell-apex heterogeneity among neighbouring cells in the same nephron of normal rats and CID^{AC} rats is confirmed [5].

(c) There are no obvious changes in the cell-coat reactivity after subjecting the animals to a CID^{AC} or a G872-CID^{VitD} treatment. The overall distribution pattern remains unchanged. But there is a relative reaction product deficiency seen at cell apices opposing intra-tubular crystals at short distance to cells.

The combination of pre-embedding lectin reaction procedures and ultrastructural preservation by a reduced osmium reaction on aldehyde-fixed Vibratome sections visualizes both aspects, provided the lectin reactive sites are extracellular. From results with single lectins, it is realized that absence of detectability of a coat reaction product does not imply its absence because a different sugar moiety not detected by that lectin can be present. Technically, this aspect is partially solved by the use of lectin mixtures (Mix4/PO), but even then our results are restricted because the specificity of only a limited number of lectins in the coat of cell types has been studied. Therefore, "absence" does not give a definitive judgement. Moreover, a clear-cut reduction of coat reactivity as reported after gentamicin treatment is not seen in our CID rats, but it may be that we studied too small section areas. Cell characterization at the LM level has, in the literature, predominantly been based on the presence of reaction product [48, 53]. However, we have the impression that once the cellular ultrastructure is introduced in combination with lectin reactivity as a parameter, a dilemma is created to which of the two priority has to be given for cell characterization. Once this dilemma is solved, previously given cell characteristics, based on a single parameter, may have to be reconsidered.

In RCM, the intrinsic cell contrast greatly improves the visibility of cell details (Figs. 1, 2, 3, 4, 9 and 10) and shows a parallel between electron- and light-scattering capacity. The presence of lectin/PO/$Os^{VI}Fe^{II}$ reaction products in apical cell coats is seen as increased intensity both in images of pre-embedding and of a lectin/PO post-embedding procedure (compare Figs. 1, 2, 3 and 4 with Figs. 17 and 18). But contrast differences in, e.g., post-embedding WGA/Au-10 nm procedures need further investigation to differentiate between the acquired lysosomal reaction product (as deduced from a PO/Au-10 nm reaction product in Figs. 19 and 20) and the intrinsic contrast of that structure. Here, we emphasized the detectability of the reaction product in the clefts between cell apices and crystals and mentioned the other localizations in passing. However, it is realized that results from pre- and post-embedding procedures proposed to visualize the various lectin localizations (lectin/PO/$Os^{VI}Fe^{II}$, lectin/PO/Au-10 nm, lectin/PO/Pt and αOPN/Au-10 nm) by RCM/LM and TEM are used as if their results are interchangeable, which may not be the case. This needs a more detailed study to be able to draw conclusions, e.g., about the cellular lectin production sites. The same holds for our observations about the reactivity with the various crystals. Double labelling procedures are needed to demonstrate the co-occurrence of two reaction products in the same crystal. The now scarcely-used reaction with potassium platinum hexachloride might be useful for contrast differentiation both for RCM and TEM. It has been shown before by X-ray microanalysis [12], that application of a reduced osmium reaction improves the electron-scattering capacity of the poly-DAB-reaction product, while sacrificing its selectivity [10, 11], whereas application of potassium platinum hexachloride improves only the electron-scattering capacity of the poly-DAB. The presently used metal-enhanced reagent plus reduced osmium complex combines all in one. Although reduced osmium ferrocyanide complex without a DAB reaction does not contrast lectin-containing sites, for a more selective PO reaction product discrimination, cytochemical procedures to detect poly-DAB related elements with electron energy-loss spectroscopy are required. Recently, the presence of an intra-mitochondrial platinum/PO reaction product has been confirmed by electron probe X-ray microanalysis [30], but unfortunately, platinum and osmium are elements difficult to detect by electron energy-loss imaging.

Positive answers to question (3), (4), (5) and (6) can be formulated as follows:

(d) Crystals are partially preserved by application of

a lectin/PO pre-embedding procedure.

(e) Intratubular crystals have a lectin/PO/($Os^{VI}Fe^{II}$) positive peripheral coat and reaction product inside the crystal ghosts, which in some places is continuous with unremoved crystalline CaOx, but coat material is hard to visualize at the attachment sites proper following pre-embedding procedures.

(f) After application of a post-embedding lectin/PO RCM or a lectin/Au-10 nm-TEM procedure on Lowicryl sections, lectin-related Au-10 nm-particles located in crystal/cell boundary clefts at crystal attachment sites both in CID^{AC} and CID^{VitD} rats confirm the coat's presence there. Reaction products are also detected in crystal-free cell coats, inside crystals, at the crystal's periphery and inside tubular lining cells.

(g) After a post-embedding procedure, WGA/Au-10 nm-reactivity is also seen at the ultrastructural level at similar sites on sections from a WGA/PO pre-embedding procedure.

(h) Similarly, reaction products are observed around and inside free-floating intratubular and retained and overgrown crystal agglomerates by αOPN/PO or αOPN/Au-10 nm reactions, used comparatively to lectin-related crystal matrix characterization.

In spite of the newly presented ultrastructural observations, question (4) is difficult to answer. The role of the apical coat in the events of the crystal/cell coat interactions during or shortly after the interaction remains obscure and needs further investigation.

On one hand, in pre-embedding procedures, situations are encountered in which a lectin-positive apical coat is present in the vicinity of just attached (?) crystals (Fig. 11). But, in the exotubulosis process, where crystals are being removed from the tubular lumen by cells embracing it (Figs. 10 and 16) in the cleft between crystal and cell apex, no reaction product is present. It can be speculated that the latter cells are lacking a coat once the crystal for the first time encountered the cell apex, but certainty cannot be obtained. Once the crystals are completely overgrown by the neighbouring epithelial cells, lectins are prevented from reaching the crystal/cell clefts, which is a known disadvantage of a pre-embedding procedure. Because after post-embedding procedures, WGA/Au-10 nm reaction products are seen at these clefts (Figs. 19 and 20); this seems to confirm the presence of a lectin-penetration artefact and to exclude the absence of a cell coat before attachment, although it is hard to differentiate in the post-embedding procedure between reaction product on a peripheral coat of the crystal and on the cell coat.

On the other hand, crystals are seen in the vicinity of the cell apices at sites where coat material is relatively faintly contrasted at the microvilli (compare Fig. 4 with Figs. 10, 11 and 12). When larger crystals apparently are attached to the cell apex, some cell apices show a relative reaction product reduction, but positive coat material is detectable (Fig. 10) around the crystals. In addition, cell apex adaptations by broadening of the villi are seen, which are reaction product negative (Figs. 12 and 13). Hence, because a coat is faintly present, it can be speculated that crystal/cell interaction is more guided by relative quantitative changes in the coat material than by its complete absence.

Recently, dynamic interaction studies between crystals and cultured cells on porous or solid supports have led to the observation that under "static conditions" a mathematical relation can be found for this crystal/cell interaction [49, 50, 60, 61, 71]. From these observations, a crystal-binding site theory has been postulated, which has been correlated with the absence or presence of lipid membrane compounds [51]. We would like to emphasize that, under such conditions, coat material can be an intermediary in this process.

Recent results [27, 39] indicated that under cell culture conditions, both high oxalate concentrations and the presence of crystals in a static incubation model caused serious cell damage as measured by the excretion into the incubation fluid of cellular enzymes. Cells damaged among other agents, e.g., by high oxalate concentrations, might also have altered coats prone to interact with crystals and stimulate gene expression [28]. Such cells might desquamate into the lumen and cover the free-floating crystals (Fig. 10).

On the other hand, calculations [33, 46, 47] using a dynamic model have shown that the speed of crystal transport through the various parts of the nephron, though different for each part, is rather high when the presence of distally located luminal speed-reducing obstructions are not taken into account. These results may make crystal/cell interaction a rather **random** process in which crystals might be retained that just bump into the cell coat (Fig. 18). These results have recently been criticized by Söhnel *et al.* [65] with respect to the role of agglomeration in papillary stone formation and where stones start to grow: inside the ducts of Bellini or outside on the papilla. Our recent rat model results on crystal enrobing at the papillary periphery and the present results (Figs. 19, 20, 21, 22, 23, 24 and 25) seem to indicate that single crystals in the core of such stones (Fig. 3, [65]) have to be considered as conglomerates of nanometer-sized crystals when observed at the ultrastructural level [23].

The cell membrane damaging character of uncoated exogenous COM crystals [20] and the ultrastructural presence of membranous material around and inside endogenous crystals has been demonstrated [23, 36, 37] in tissues in which the crystalline material had been removed by the applied preparative procedure. In the

present study, with partially preserved crystals, it is demonstrated (Figs. 12 and 13) that intratubular crystal ghosts at the outside are covered by a Mix4/PO positive reaction product. A similar reaction product is seen decorating retained crystals in G872 treated CID^{VitD} rats (Figs. 14 and 15). It can be speculated that the presence of G872 during the CID^{VitD} treatment has amplified the cell- and crystal-coat reactivity. But, differences between CID^{AC} and CID^{VitD} and the aspect of "coat-damage restoration" after G872 treatment needs a further quantitative investigation to be conclusive.

We have previously [14] shown that after prolonged post-fixation, crystals are removed, and two situations are encountered: crystals with and without a residual internal structure. It has been discussed that the latter situation might be dangerous to interpret because a preparation artefact is present. In the present study, which confirms these observations, that problem is circumvented by a shorter post-fixation resulting in partial crystal preservation, though at the cost of a less undisturbed microscopical registration on irradiation.

The presence of WGA/Au-10 nm and αOPN/Au-10 nm positive reaction products in a crystal matrix confirms our previous morphological observations and those recently shown by Khan [36, 37]. The presence of a lectin-positive decoration at the outside of the crystals and in a matrix leading to centrally located preserved crystalline material (Figs. 12, 13, 19, 20 and 21) reenforces the idea of recurrent crystal opsonization described previously [14]. It emphasizes the presence of secreted glycoproteins in this morphological entity and of the (proteinaceous) material with which αOPN forms a reaction product (Figs. 22, 23, 24 and 25).

The presence of urinary (proteinaceous) substances interacting with crystals as crystallization promotion/inhibition, demonstrated by others [24, 29, 54, 55, 64, 67] will not be discussed in detail here. The presented, *in situ*, ultrastructural immune-cytochemical reactions confirm their presence and show some of their characteristics. However, crystal matrices from human sources remain to be studied in detail. Although matrix proteins from human stones have been isolated and characterized [2, 36], it remains to be demonstrated whether crystal and stone matrix are immunocytochemically alike.

However, aspects of dissolution of inorganic parts from crystals during the various steps of the procedures and preservation of reactivity of the undissolved crystal parts also needs additional attention. We did not apply the well known steps to remove the crystalline material out of fear of blocking reactivity. Storage of the aldehyde-fixed material can induce (slow) dissolution of inorganic components, maintaining the total crystal integrity due to (the assumed) fixation of the organic part (Figs. 9, 14 and 15). Part of the presently used material has now been stored for over two years in a cacodylate buffer. When dissolution in the non-aqueous phases is considered to be minimal, inorganic dissolution may also occur during the aqueous immunocytochemical reactions applied to the thin sections, and reactivity then exposed may create reaction sites in the section surface. We did not use antigen retrieval steps.

Previously, it has been discussed [14, 16, 17] that the presence of coat or membranous material around the presence of a matrix inside the intratubular crystals is a reflection of a time- and/or place-dependent process. In this process, the balance between the purely inorganic (nm- to μm-sized) crystal formation and/or crystal agglomeration and its intratubular opsonization with secreted (glyco)proteins and membranes is constantly shifted backwards and forwards, leading to rather different crystal aspects in cross-section. The crystal retention process may be influenced by such rather subtle differences in the coat at the crystal exterior or the changes of the cellular apical coat material due to fluctuations in coat secretion and liberation into the tubular lumen or other environmental circumstances, such as recently demonstrated in the static model [50].

Although αOPN/Au-10 nm is mainly used in this study to compare the character of crystal matrix proteins with WGA-reactivity at these sites, our observations as such (Figs. 23, 24 and 25) demonstrate its interference with (inorganic) CaOx crystals reported before [1, 31, 62] and with hydroxyapatite [25]. This may confirm the "normal" inhibitory reaction to nucleation of calcium oxalate, as recently proposed by Worcester, Kleinman, Blumenthal and Beshenky [72, 73, 74] judged here from its presence around nm- and μm-sized crystal ghosts in the large free-floating intratubular and just-retained crystal agglomerates.

In normal rat kidney, the production and excretion of OPN is reported to be located in the loop of Henle [44] where it may assist in inhibition of nucleation. However, Kohri *et al.* [45] recently demonstrated, by comparing *in situ* hybridization for OPN mRNA in kidneys from control and (glyoxylic) stone-forming rats, reaction product to be clearly located in distal tubular and collecting duct cells and not in proximal tubules and glomeruli. An increase in OPN mRNA expression in distal tubules and collecting duct cells correlated with the duration and dosage of their crystal induction protocol. A 5.2-fold increase over control rats for the OPN mRNA for the glyoxylic acid induction pyelonephritis model and a 2.3-fold increase in the vitamin D_3 induced hydronephrose model was demonstrated by Umekawa *et al.* [69, 70], but upregulation was not found in gentamicin induced damage in proximal tubular cells. We have a single observation of a heavily αOPN/Au-10 nm decorated Golgi vesicle in an epithelial cell apex to which

a crystal agglomerate was attached (not shown), whereas the αOPN/Au-10 nm decorated crystal agglomerate shown in Figure 23 was located below an epithelial cell with a WGA-positive cell coat from the pre-embedding reaction procedure. Upregulation of OPN expression is also reported after deliberate induction of ischemia in rat kidneys [18, 44] and after myocardial infarction [22]. The OPN reaction in intratubular and retained crystals may also indicate the presence of tissue damage and/or macrophage activity stimulation, here induced by our CID treatments.

Acknowledgements

The financial support of the Dutch Kidney Foundation (E.R. Boevé, R. de Water and P.P.M.C. van Miert, grant 92. 1235) and the SUWO (Stichting Urologisch Wetenschappelijk Onderzoek) is acknowledged.

References

[1] Asplin J, Hoyer JR, Nakagawa Y, Coe FL (1992) Uropontin (UP) inhibits calcium oxalate monohydrate (COM) crystal growth and nucleation. J Am Soc Nephrol **3**: 669-672.

[2] Binette JP, Binette MB (1994) Sequencing of proteins extracted from stones. Scanning Microsc **8**: 233-240.

[3] Boevé ER, Ketelaars GAM, Vermey M, Cao LC, Schröder FH, de Bruijn WC (1993) An ultrastructural study of experimentally induced microliths in rat proximal and distal tubules I. J Urol **149**: 893-899.

[4] Boevé ER, Cao LC, Verkoelen CF, Romijn JC, de Bruijn WC, Schröder FH (1993) Glycosaminoglycans and other sulphated polysaccharides in calculogenesis of urinary stones. World J Urol **12**: 43-48.

[5] Brown D, Roth J, Orci L (1985) Lectin gold cytochemistry reveals intercalated cell heterogeneity along rat kidney collecting ducts. Am J Physiol **248** (Cell Physiol **17**): C348-C356.

[6] Cao LC, Boevé ER, Schröder FH (1991) The mechanisms of action of glycosaminoglycans (GAG's) in calcium oxalate stone prevention. A review. J Lithotripsy Stone Dis **3**: 324-333.

[7] Cao LC, Boevé ER, Schröder FH, Robertson WG, Ketelaars GAM, de Bruijn WC (1993) The effect of two new semi-synthetic glycosaminoglycans (G871, G872) on the zeta-potential of calcium oxalate crystals and on growth and agglomeration. J Urol **147**: 1643-1646.

[8] de Bruijn WC (1973) Glycogen, its chemistry and morphologic appearance in the electron microscope I. A modified OsO_4 fixative which selectively contrasts glycogen. J Ultrastruct Res **42**: 29-44.

[9] de Bruijn WC (1995) Contrast-staining with reduced osmium complexes. J Histochem Cytochem **43**: 965-966.

[10] de Bruijn WC, van Buitenen JMH (1980) X-ray microanalysis of aldehyde-fixed glycogen contrast stained with Os(VI)Fe(II) and Os(VI)Ru(IV) complexes. Histochem Cytochem **28**: 1242-1249.

[11] de Bruijn WC, van Buitenen JMH (1981) X-ray microanalysis of non-aldehyde-fixed glycogen contrast stained with $Os(VIII)O_4$, Os(VIII)Fe(III), or Os(VI)-Fe(II) complex *in vitro*. Histochem J **16**: 125-145.

[12] de Bruijn WC, van der Meulen J, Brederoo P, Daems WTh (1986) Pt-staining of peroxidatic reaction products at ultrastructural level. Histochemistry **84**: 492-500.

[13] de Bruijn WC, Ketelaars GAM, Boevé ER, Sorber CWJ, Cao LC, Schröder FH (1993) Electron energy-loss spectroscopical and image analysis of experimentally induced microliths II. J Urol **149**: 900-905.

[14] de Bruijn WC, Boevé ER, van Run PRWA, van Miert PPMC, Romijn JC, Verkoelen CF, Cao LC, Schröder FH (1994) Etiology of experimental calcium oxalate monohydrate nephrolithiasis in rats. Scanning Microsc **8**: 541-550.

[15] de Bruijn WC, Boevé ER, Cao LC, Verkoelen CF, Romijn JC, Schröder FH (1994) Formation and role of intracellular crystals in urolithiasis. In: Urolithiasis, Consensus and Controversies. Rao PN, Kavanagh JP, Tiselius H-G (eds.). South Manchester Univ. Hospitals, Manchester, England. pp. 23-28.

[16] de Bruijn WC, Boevé ER, van Run PRWA, van Miert PPMC, de Water R, Romijn JC, Verkoelen CF, Cao LC, Schröder FH (1995) Etiology of calcium oxalate nephrolithiasis in rats. I. Can this be a model for human stone formation? Scanning Microsc **9**: 103-114.

[17] de Bruijn WC, Boevé ER, van Run PRWA, van Miert PPMC, de Water R, Romijn JC, Verkoelen CF, Cao LC, van 't Noordende JM, Schröder FH. (1995) Etiology of calcium oxalate nephrolithiasis in rats. II. The role of the papilla in stone formation. Scanning Microsc **9**: 115-125.

[18] Denhart DT, Lopez CA, Rollo EE, Hwang SM, An XR, Walther SE (1995) Osteopontin-induced modifications of cellular functions. In: Annals of the New York Academy of Science. Vol. 760. Denhart DT, Butler WT, Chambers AF, Senger DR (eds.). pp. 127-141.

[19] de Water R, de Bruijn WC, Boevé ER, van Run PRWA, van Miert PPMC, Vermaire CP, Romijn JC, Verkoelen CF, Cao LC, Schröder FH (1996) Pathological and immunocytochemical changes in chronic calcium oxalate nephrolithiasis in rat. Scanning Microsc **10**, 577-590.

[20] Elferink JGR, Deierkauf M (1987) Enzyme release from polymorphonuclear leukocytes during interaction with calcium oxalate microcrystals. J Urol **138**: 164-167.

[21] Finlayson B, Reid F (1978) The expectation of free and fixed particles in urinary stone disease. Invest Urol **15**: 442-448.

[22] Giachelli CM, Liaw L, Murry, CE, Schwarz SM, Almeida M (1995) Osteopontin expression in cardiovascular diseases. In: Annals of the New York Academy of Science. Vol. 760. Denhart DT, Butler WT, Chambers AF, Senger DR (eds.). pp. 109-126.

[23] Gill WB, Ruggierro KJ, Strauss FH (1979) Crystallization studies in a urothelium lined living test tube (the catheterized female rat bladder). Invest Urol **17**: 257-261.

[24] Gokhale JH, Glenton PA, Khan SR (1994) Analysis of Tamm Horsfall protein in a rat model of nephrolithiasis. In: Urolithiasis, Consensus and Controversies. Rao PN, Kavanagh JP, Tiselius H-G (eds.). South Manchester Univ. Hospitals, Manchester. pp. 402-403.

[25] Goldberg HA, Hunter GK (1995) The inhibitory activity of osteopontin on hydroxyapatite formation *in vitro*. In: Annals of the New York Academy of Science. Vol. 760. Denhart DT, Butler WT, Chambers AF, Senger DR (eds.). pp. 305-308.

[26] Grases F, Costa-Bauzá A, Conte A (1993) Studies on structure of calcium oxalate monohydrate renal papillary calculi. Mechanism of formation. Scanning Microsc **7**: 1067-1074.

[27] Hackett RL, Shevock PV, Khan SR (1990) Cell injury associated calcium oxalate crystalluria. J Urol **144**: 1535-1545.

[28] Hammes M, Lieske JC, Pawar S, Spargo BH, Toback FG (1995) Calcium oxalate monohydrate crystals stimulate gene expression in renal epithelial cells. Kidney Int **48**: 501-509.

[29] Hess B (1994) Tamm Horsfall Mucoprotein. In: Urolithiasis, Consensus and Controversies. Rao PN, Kavanagh JP, Tisselius H-G (eds.). South Manchester Univ. Hospitals, Manchester. pp. 119-123.

[30] Hiraoka T, Hirai K (1995) Cytochrome oxidase activity of individual mitochondria as quantified by platinum-diaminibenzidine reaction with energy dispersive X-ray analyzer. Acta Histochem Cytochem **28**: 247-254.

[31] Hoyer JR, Otvos L, Urge L (1995) Osteopontin in stone formation. In: Annals of the New York Academy of Science. Vol. 760. Denhart DT, Butler WT, Chambers AF, Senger DR (eds.). pp. 257-265.

[32] Iványi B, Steen Olsen T (1991) Immunohistochemical identification of tubal segments in percutaneous renal biopsies. Histochemistry **95**: 351-356.

[33] Jordan WR, Finlayson B, Luxenberg M (1978) Kinetics of early time calcium oxalate nephrolithiasis. Invest Urol **15**: 465-468.

[34] Khan SR (1991) Pathogenesis of oxalate urolithiasis: Lessons from experimental studies with rats. Am J Kidney Dis **17**: 398-401.

[35] Khan SR (1995) Experimental calcium oxalate nephrolithiasis and the formation of human urinary stones. Scanning Microsc **9**: 89-101.

[36] Khan SR (1995) Heterogeneous nucleation of calcium oxalate crystals in mammalian urine. Scanning Microsc **9**: 597-616.

[37] Khan SR (1995) Calcium oxalate crystal interaction with renal tubular epithelium, mechanism of crystal adhesion and its impact on stone development. Urol Res **23**: 71-79.

[38] Khan SR, Hackett RL (1991) Retention of calcium oxalate crystals in renal tubules. Scanning Microsc **5**: 707-712.

[39] Khan SR, Hackett RL (1993) Hyperoxaluria, enzymuria and nephrolithiasis. In: Kidney, Proteins and Drugs: An Update. Biachi C, Bocci V, Caronne FA, Rabkin R (eds.). Karger, Basel, Switzerland. Contrib Nephrol, Vol 101. pp. 190-193.

[40] Khan SR, Finlayson B, Hackett RL (1979) Histology study of the early events in oxalate induced intranephronic calculosis. J Urol **17**: 199-202.

[41] Khan SR, Finlayson B, Hackett RL (1982) Experimental calcium oxalate nephrolithiasis in the rat. The role of the renal papilla. Am J Pathol **107**: 59-69.

[42] Khan SR, Shevock PN, Hackett RL (1989) Urinary enzymes and calcium oxalate urolithiasis. J Urol **142**: 840-849.

[43] Khan SR, Shevock PN, Hackett RL (1992) Acute hyperoxaluria, renal injury and calcium oxalate urolithiasis. J Urol **147**: 226-230.

[44] Kleinman JG, Worcester EM, Behensky AM, Sheridan AM, Bonventre JV, Brown D (1995) Upregulation of osteopontin expression by ischemia in rat kidney. In: Annals of the New York Academy of Science. Vol. 760. Denhart DT, Butler WT, Chambers AF, Senger DR (eds.). pp. 321-324.

[45] Kohri K, Nomura S, Kitamura Y, Nagata T, Yoshioka K, Igichi M, Yamata T, Umakawa T, Suzuki Y, Sinohara H, Kurita T (1993) Structure and expression of the mRNA encoding urinary stone protein (Osteopontin). J Biol Chem **268**: 15180-15184.

[46] Kok DJ (1996) Crystallization and stone formation inside the nephron. Scannning Microsc **10**, 471-486.

[47] Kok DJ, Khan SR (1994) Chances for a free or fixed particle mechanism. In: Urolithiasis, Consensus and Controversies. Rao PN, Kavanagh JP, Tisselius H-G (eds.). South Manchester Univ. Hospitals, Manchester. pp. 431-432.

[48] Krenács T, Krenács L, Bozóky B, Iványi B (1990) Double and triple immunocytochemical labelling at the light microscope level in histopathology. Histochem J **22**: 530-536.

[49] Lieske JC, Toback FG (1993) Regulation of

renal epithelial cell endocytosis by calcium oxalate monohydrate crystals. Am J Physiol **264**: F800-F807.

[50] Lieske JC, Leonard R, Toback FG (1995) Regulation of calcium oxalate monohydrate crystals to renal epithelial cells is inhibited by specific anions. Am J Physiol **268**: F604-F612.

[51] Mandel N (1994) Crystal-membrane interaction in kidney stone disease. J Am Soc Nephrol **5**: 37-45.

[52] Mijan, JL, Aneiros J, O'Valle F, Zuloaga A, Martinez JL, Camara M (1988) Experimental oxalosis in rats: An electron microscopic study. Urol Int **43**: 19-23.

[53] Nadasdy T, Lazik S, Block KE, Johnson DL, Silva FG (1994) Tubular atrophy in the end-stage kidney: A lectin and immunohistochemical study. Human Pathol **25**: 22-28.

[54] Nakagawa Y, Abram V, Kézdy F, Kaiser ET, Coe FL (1983) Purification and characterization of the principal inhibitor of calcium oxalate monohydrate crystal growth in human urine. J Biol Chem **258**: 12594-12600.

[55] Netzer M (1994) Nephrocalcin. In: Urolithiasis, Consensus and Controversies. Rao PN, Kavanagh JP, Tiselius H-G (eds.). South Manchester Univ. Hospitals, Manchester. pp. 125-128.

[56] Nouwen EJ, Verstrepen WA, Buyssens N, Zhu M-Q, De Broe ME (1994) Hyperplasia, hypertrophy, and phenotypic alterations in the distal nephron after acute proximal tubular injury in the rat. Lab Invest **70**: 479-493.

[57] Parsons CL (1994) A model for the function of glycosaminoglycans in the urinary tract. World J Urol **12**: 38-42.

[58] Parsons CL, Danielson B, Fellström B (1985) Inhibition of sodium urate crystal adherence to bladder surface by polysaccharide. J Urol **134**: 614-616.

[59] Prins FA, van Diemen-Steenvoorde R, Bonnet J, Cornelese-ten Velde J (1993) Reflection contrast microscopy of ultrathin sections in immunocytochemical localization studies: A versatile technique bridging electron microscopy with light microscopy. Histochemistry **99**: 417-425.

[60] Riese RJ, Mandel NS, Wiessner JH, Mandel GS, Becker CG, Kleinman JG (1982) Cell polarity and calcium oxalate crystal adherence to cultured collecting duct cells. Am J Physiol **262**: F177-F184.

[61] Riese RJ, Riese WJ, Kleinman JG, Wiessner JH, Mandel GS, Mandel NS (1988) Specificity in calcium oxalate adherence to papillary epithelial cells in culture. Am J Physiol **255**: F1025-F1032.

[62] Shiraga H, Min W, van Dusen WJ, Clayman MD, Miner D, Terrel CH, Sherbotie JR, Foreman JW, Przysiecki C, Neilson EG, Hoyer JR (1995) Inhibition of calcium oxalate crystal growth *in vitro* by uropontin: Another member of the aspartic acid-rich protein superfamily. Proc Natl Acad Sci **89**: 426-430.

[63] Silva FG, Nadasdy T, Laszik S (1993) Immunohistochemical and lectin dissection of the human nephron in health and disease. Arch Pathol Lab Med **117**: 1233-1239.

[64] Sirivongs D, Nakagawa Y, Vishny WK, Favus MJ, Coe FL (1989) Evidence that mouse renal proximal tubule cells produce nephrocalcine. Am J Physiol **26**: F390-F398.

[65] Söhnel O, Grases F, Garcia-Ferragut L (1994) Role of agglomeration in the early stages of papillar stone formation. Scanning Microsc **8**: 513-522.

[66] Sorber CWJ, van Dort JB, Ringeling PC, Cleton-Soeteman MI, de Bruijn WC (1990) Quantitative energy-filtered image analysis in cytochemistry. II. Morphometric analysis of element distribution images. Ultramicroscopy **32**: 69-79.

[67] Stapleton AMF, Ryall RL (1994) Novel developments of a specific antibody to prothrombin fragment 1. Crystal matrix protein exposed as an F1 alias. In: Urolithiasis, Consensus and Controversies. Rao PN, Kavanagh JP, Tiselius H-G (eds.). South Manchester Univ. Hospitals, Manchester. pp. 404-405.

[68] Truong LD, Phung VT, Yoshikawa Y, Mattioli CA (1988) Glycoconjugates in normal human kidney. A histochemical study using 13 biotinylated lectins. Histochemistry **90**: 51-60.

[69] Umekawa T, Kohri K, Kurita T, Hirota S, Nomura S, Kitamura Y (1995) Expression of osteopontin messenger RNA in the rat kidney on experimental model of renal stone. Biochem Mol Biol Int **35**: 223-230.

[70] Umekawa T, Yamate T, Amasaki N, Kohri K, Kurita T (1995) Osteopontin mRNA in the kidney on an experimental rat model of renal stone formation without renal failure. Hauri D (ed.). Karger, Basel. Urol Int, Vol. 55. pp. 6-10.

[71] Verkoelen CF, Romijn JC, de Bruijn WC, Boevé ER, Cao LC, Schröder FH (1995) Association of calcium oxalate monohydrate crystals with MDCK cells. Kidney Int **48**: 129-138.

[72] Worcester EM, Beshensky AM (1995) Osteopontin inhibits nucleation of calcium oxalate crystals. In: Annals of the New York Academy of Science. Vol. 760. Denhart DT, Butler WT, Chambers AF, Senger DR (eds.). pp. 375-377.

[73] Worcester EM, Blumenthal SS, Beshensky AM (1992) The calcium oxalate crystal growth inhibitor protein produced by mouse kidney cortical cells in culture is osteopontin. J Bone Miner Res **7**: 1029-1036.

[74] Worcester EM, Kleinman JG, Beshensky AM (1995) Osteopontin production by cultured kidney cells. Annals of the New York Academy of Science. Vol. 760. Denhart DT, Butler WT, Chambers AF, Senger DR (eds.). pp. 266-278.

[75] Zondervan PE, van der Kwast ThH, de Jong A, Visser WJ, de Bruijn WC (1986) Lysosomal localization of secretory prostatic acid phosphatase in human hyperplastic prostate epithelium. Urol Res **14**: 331-335.

Discussion with Reviewers

R.L. Hackett: (1) The authors discuss the attachment of crystals to the cell coat as a factor of retention, but it would seem that it is more a matter of crystal aggregation into the matrix. In terms of retention, what is the role the basement membrane in this model? (2) Do lectins adhere to native crystals? *In vivo*, crystals always acquire a biological coating. Have the authors done any control *in vitro* studies to determine whether the lectins they tested would coat pre-formed calcium oxalate crystals? Could it be possible that the lectins are reacting to the coated crystals rather than the crystal itself?

Authors: These are interesting aspects we have not considered during the interpretation of our results. We think it depends on the position one takes towards the question about which entity is the most important one for retention: (a) the large circulating crystal as a whole; (b) the microcrystals enclosed, forming this aggregate; (c) the component that glues these microcrystals together; or (d) coat material in the cell apices. We started to study the relation between (a) and (d), and ended up by demonstrating (in line with our previous observations and those from your group [38]) that large crystals are composed of microcrystals and other components. We did not perform *in vitro* studies to determine whether the lectins tested would coat pre-formed calcium oxalate crystals. We assumed that lectins do not react with inorganic crystals. Whereas, inorganic crystal coating with complex sugars, to which the lectins do react, was considered not so easy to perform.

But, on inspecting Figures 23 and 24, we think an answer to your questions can be given. In these figures, partially preserved microcrystals are surrounded by substances detected by the applied cytochemical procedure. Microcrystals, of sizes varying from several nanometers to micrometers, are individually coated. When two microcrystals are seen together inside this large crystal, coat is facing coat. However, at the periphery of circulating large crystals, the situation might be different. When there exist circulating coated microcrystals, which are hard to detect as free-floating entities, coat to coat interaction can induce aggregation on the crystal surface and on the cell apices or on both, cementing micro- or large crystals to (similarly or differently coated?) cell apices. Incorporation into "the crystal matrix," as suggested in your question, remains still to be demonstrated. We showed the occurrence and suggested a possible co-occurrence of the two detected substances around microcrystals. When, by multiple labellings experiments, several substances are demonstrated to be colocalized, they can form together "a crystal matrix." We agree that the existence of a crystal matrix is likely because morphologically it is seen inside such large retained crystals after removal of the inorganic fraction, shown in papers by Khan [36], by us [14] and, immunocytochemically, by McKee *et al.* [76].

When there exist uncoated microcrystals, apical complex sugars may attract such entities to their coats. The variation in microcrystal sizes suggests the existence of uncoated COM microcrystals during periods of time travelling along the nephron, before coating occurs.

The role of basement membranes remains obscure. We are aware of papers showing desquamation of tubular cells, leading to denuded basement membranes and the presence of crystals claimed to be attached to them. Cell desquamation has not been so frequently observed in our material, possibly due to the fact that we allow rats, after the crystal induction period, 1-3 days of recovery, which may lead to repair of the tubular integrity. Previously, basement membrane production has been reported by us to occur in the process of exotubulosis. Retained crystals are overgrown by epithelial cells (Fig. 23) that deposit new basement membrane material between the crystal surface and cells.

H-G Tiselius: Can the authors exclude the disappearance of coating material during the preparation as an explanation of the heterogeneous reactivity?

Authors: No, we cannot. We were somewhat surprised by the observed heterogeneous reactivity. This always induces the question: absence of material or absence of reactivity? We explained it initially in terms of absence of reactivity for the particular lectin applied, which led to the use of the lectin-mixture. The other option was damage by the applied stone inducing diet. But there were insufficient observations to support that idea firmly because heterogeneous reactivity was also seen in the untreated rats. Another option was that coats were absent or non-reacting, either as a consequence of the cell cycle (juvenile or senescent) or, suggested by your question, because the coat material of that particular cell was less preserved or not preserved during tissue processing.

Additional References

[76] McKee MD, Nanci A, Khan SR (1995) Ultrastructural immunodetection of osteopontin and osteocalcin as major matrix components of renal calculi. J Bone Miner Res **10**: 1913-1929.